Modeling of a Hybrid Electric Vehicle Powertrain Test Cell Using Bond Graphs

Mariano Filippa, *Student Member, IEEE*, Chunting Mi, *Senior Member, IEEE*, John Shen, *Senior Member, IEEE*, and Randy C. Stevenson

***Abstract*—A Bond Graph model of a hybrid electric vehicle (HEV) powertrain test cell is proposed. The test cell consists of a motor/generator coupled to a HEV powertrain and powered by a bidirectional power converter. Programmable loading conditions, including positive and negative resistive and inertial loads of any magnitude are modeled, avoiding the use of mechanical inertial loads involved in conventional test cells. The dynamics and control equations of the test cell are derived directly from the Bond Graph models. The modeling and simulation results of the dynamics of the test cell are validated through experiments carried out on a scaled-down system.**

***Index Terms*—Bond Graphs, hybrid electric vehicle (HEV), mechatronics, modeling, powertrain test cell, road vehicle control, road vehicle electric propulsion, road vehicle electronics, road vehicle testing, simulation.**

I. Introduction

HYBRID ELECTRIC VEHICLES (HEV) are propelled by an internal combustion engine (ICE) and an electric motor/generator (EM) in series or parallel configurations. The ICE provides the vehicle an extended driving range, while the EM increases efficiency and fuel economy by regenerating energy during braking and storing excess energy from the ICE during coasting. Design and control of such powertrains involve modeling and simulation of intelligent control algorithms and power management strategies, which aim to optimize the operating parameters to any given driving condition.

Traditionally there are two basic categories of HEV, namely series hybrids and parallel hybrids [1]. In series HEV, the ICE mechanical output is first converted to electricity using a generator. The converted electricity either charges the battery or bypasses the battery to propel the wheels via an electric motor. This electric motor is also used to capture the energy during braking. A parallel HEV, on the other hand, has both the ICE and an electric motor coupled to the final drive shaft of the wheels via clutches. This configuration allows the ICE and the electric motor to deliver power to drive the wheels in combined mode, or ICE alone or motor alone modes. The electric motor is also used for regenerative braking and for capturing the excess energy of the ICE during coasting. Recently, series-parallel and complex HEV have been developed to improve the power performance and fuel economy [2].

The HEV powertrain design process is aided by modeling and simulation. Several models and control algorithms were proposed and implemented [3]–[6]. Issues such as battery modeling, torque management, control algorithms and vehicle simulation, were addressed by using simulation tools such as Matlab/Simulink. Computer models are readily available for these purposes [7].

Due to the complexity involved in the operation of HEVs, prototypes must be validated by testing through alternative drive cycle scenarios. This testing is usually performed in laboratory dynamometers with the capability of recreating road load conditions and measuring the performance of different control strategies [8], [9]. This paper proposes a test cell capable of reproducing inertial and resistive loads of any magnitude. The model and control equations of the powertrain and the test cell are developed and simulated using Bond Graphs.

Created by Paynter in 1959, Bond Graphs are a graphical tool used to describe and model subsystem interactions involving power exchange [10]. This formulation can be used in hydraulics, mechatronics, thermodynamic and electrical systems. Bond Graph has been proven effective for the modeling and simulation of multidomain systems [11]–[14] including automotive systems [15]–[24]. Bond Graphs were also used to model a hybrid electric vehicle drivetrain [25]. Dynamic models for each of the drivetrain components were presented, including ICE, transmission, chassis/body, battery, and ac induction motor.

Developing the model of the test cell with Bond Graphs provides the ability to interface the test cell directly with the models used in the design stage. Road models and loading parameters are inputs to the test cell model. Simulation results of powertrain torque and speed are presented in the paper. Experiments were carried out on a scaled-down setup using a 2 kW dc motor and a 2-kW induction motor. The test results of powertrain torque and powertrain speed matches the simulation results, therefore, validated the proposed model.

II. Introduction to Bond Graph Modeling

In a Bond Graph model, a physical system is represented by basic passive elements that are able to interchange power: *resistances* (R), *capacitances* (C), and *inertias* (I). Although these names suggest a direct application in electrical systems, they are

Manuscript received October 1, 2004; revised December 14, 2004 and January 30, 2005. This work was supported by the Center for Engineering Education and Practice (CEEP) Grant and the Rackham Grant from the University of Michigan. The review of this paper was coordinated by Prof. A. Emadi.

M. Filippa is with the General Electric Company, Salem, VA 24153 USA (e-mail: mariano.filippa@ge.com).

C. Mi is with the Department of Electrical and Computer Engineering, University of Michigan, Dearborn, MI 48128 USA (e-mail: chrismi@umich.edu).

J. Shen is with the Department of Electrical and Computer Engineering, University of Central Florida, Orlando, FL 32816 USA (e-mail: johnshen@mail.ucf.edu).

R. C. Stevenson is with Visteon Corporation, Dearborn, MI 48120 USA (e-mail: rsteven7@visteon.com).

Digital Object Identifier 10.1109/TVT.2005.847226

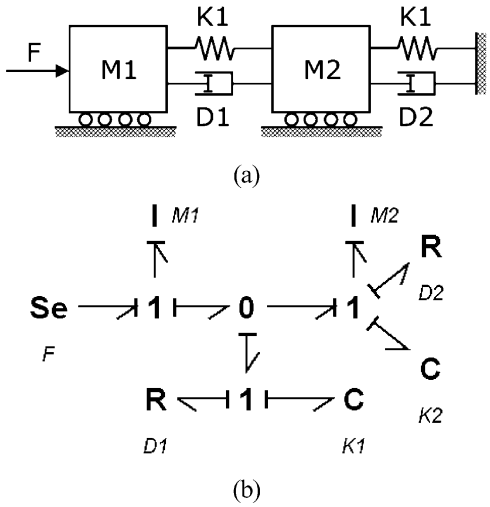

Fig. 1. A Bond Graph modeling example. (a) Schematic of a mechanical system including two masses connected by springs and mechanical dampers. (b) Bond Graph of the mechanical system.

used in any other domains as well, e.g., friction as a mechanical resistance, a compressible fluid as a capacitance and a flywheel as an inertial element.

Each element has one or more ports where power exchange can occur. This *power* (P) is expressed as a product of two variables: *effort* (e) and *flow* (f). These names are used extensively in all domains, but have a unique name on each domain: force and speed in mechanical, voltage and current in electrical, pressure and flow in hydraulics, and so on. Additional variables are defined: *momentum* (p) as the time integral of effort and *displacement* (q) as the time integral of flow.

Additional elements are needed to fully describe a system: *Sources of effort* (Se) and *Sources of Flow* (Sf) are active elements that provide the system with effort and flow, respectively; *Transformers* (TF) and *Gyrators* (GY) are two port elements that transmit power, but scale their effort and flow variables by its modulus; and *One Junction* (1) elements are multiport elements that distribute power sharing equal flow, while *Zero Junction* (0) elements distribute power, having equal effort among all ports.

Bond graph elements are linked with half arrows (bonds) that represent power exchange between them. The direction of the arrow indicates the direction of power flow when both effort and flow are positive. Full arrows are used when a parameter is to be passed between elements, but no power flow occurs.

A Bond Graph can be generated from the physical structure of the system. For example, the mechanical system shown in Fig. 1(a), which includes two masses connected by two springs and two mechanical dampers, can be modeled using Bond Graphs shown in Fig. 1(b), where each element in the Bond Graph diagram correlates to a physical entity of the system.

In Fig. 1(b), the One-Junctions represent the speed of each mass. An inertia is attached to each speed (I:M1 and I:M2). The force acts on M1, therefore a Source of Effort, is applied to the One-Junction corresponding to M1. The difference of speed between the two masses drives the spring-damper system (D1, K1) through a Zero-Junction and a One-Junction. The Zero-Junction generates the difference of speed maintaining a constant effort, while the One-Junction feeds the speed difference to both D1 and K1, and splits the effort between both elements. This is accomplished in a similar way with D2 and K2, but since the wall system has zero speed, a Zero-Junction is not needed and the elements connect directly to the One-Junction.

After the system is represented by Bond Graph elements, the next step consists of assigning the power bonds and active bonds between elements. Power bonds are assigned according to the direction of positive power flow. This power convention can be set arbitrarily.

Once the power bonds are assigned, causality must be established within the Bond Graph. This causality analysis is determined by rules described in Bond Graph theory [10]. A causal stroke located at the end of a power bond indicated that effort is the driving force to the element, while a stroke located at the beginning of the bond indicates that flow is the input to the element. For example, in Fig. 1(b), on the element $R : D1$ the causal stroke is located on the beginning of the power bond, therefore the element equation should be written as $\text{effort} = \text{function}(\text{flow})$. On the other hand, $I : M1$ has a power bond with a causal stroke at the end, therefore, its equation should be written as $\text{flow} = \text{function}(\text{effort})$.

Causality in Bond Graph models is indicated with a vertical stroke at the start or end of the bond arrow. This causal stroke establishes the cause and effect relationships between elements. Causality in Bond Graphs enables the extraction of systems dynamics equations. It also provides an insight of the dynamic behavior or the model and is useful to predict modeling problems such as algebraic loops, differential causality, and causal loops.

Bond Graph is a powerful tool to model a system involving mechanical, electrical, and electromagnetic elements such as the HEV powertrain test cell proposed in this paper.

III. The Test Cell Layout

Fig. 2 depicts the proposed test cell connected to a parallel HEV powertrain. The test cell consists of a motor/generator, capable of working in motoring and generating modes, a bidirectional power electronic converter, and a grid synchronizer connected to a three phase power supply (power grid). The test cell elements perform the following operations:

1) *Motor/generator*: coupled to the powertrain transmission, this component is able to absorb or deliver power to the transmission. Torque is adjusted to achieve the desired loading condition.
2) *Power electronic converter*: this component drives the electric motor/generator. It is able to deliver energy to the motor, as well as accepting energy from the motor. The energy delivered to the motor is taken from the power grid, while the absorbed energy is sent to the grid synchronizer.
3) *Grid synchronizer*: when the cell accepts power from the powertrain, this energy is taken from the power electronic converter and sent back to the grid. This element avoids the dissipation of high amounts of energy into heat, rendering an energy efficient test cell.
4) *Controller*: based on DSpace/DSP controllers, this component drives the power electronic converter to adjust the

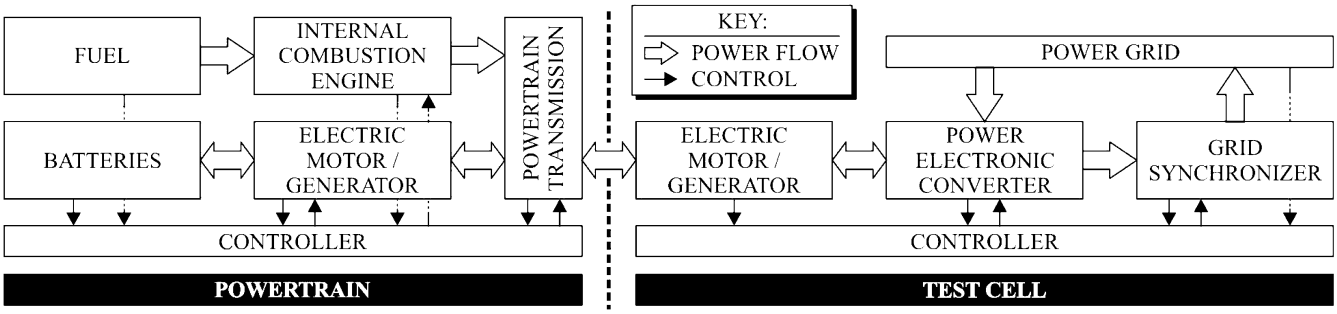

Fig. 2. Test cell layout showing a parallel hybrid powertrain connected to it. The powertrain shown has a parallel configuration with both the ICE and the motor connected to a planetary transmission. The test cell shown consists of an electric motor/generator connected to a power grid through a power converter and grid synchronizer.

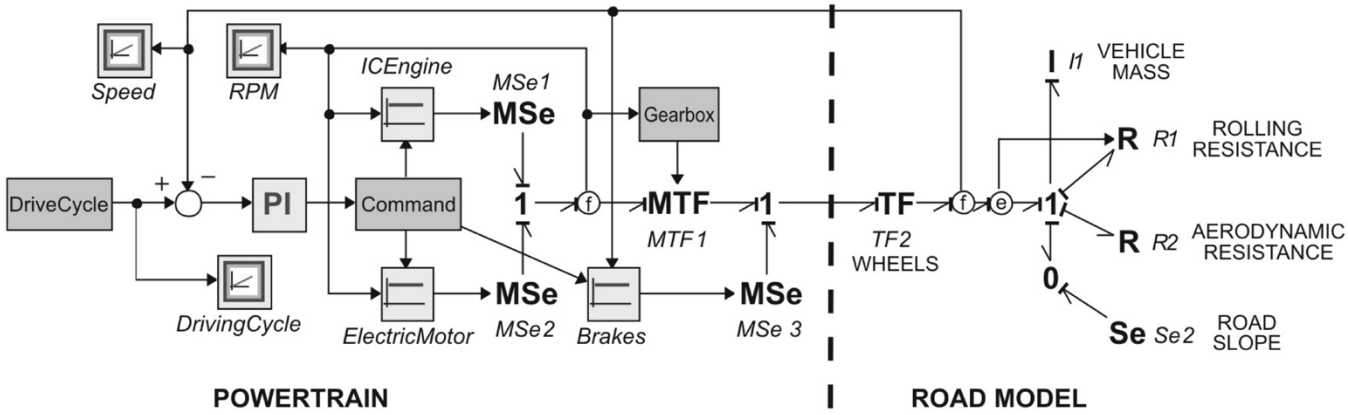

Fig. 3. HEV powertrain model connected to a simple road model.

motor/generator torque. This controller is also responsible of controlling the grid synchronizer.

The key advantages of this test cell are: a) the motor/generator can operate in either motoring or generating modes, therefore enabling the recreation of any loading condition needed, and b) most of the powertrain generated energy can be recovered and sent back to the grid, resulting in a highly energy efficient test cell.

The controller is the main component of the test cell which controls the loading applied to the powertrain. The control algorithm is obtained from the HEV powertrain and road models. These models are developed using Bond Graph methods which allow rapid extraction of control equations from the graphs.

IV. Powertrain and Road Models

Fig. 3 shows the Bond Graph model of a powertrain connected to a simple road model. The powertrain is represented by the combination of sources of effort (MSe_1, MSe_2, and MSe_3). These sources represents the torque produced by the ICE, the motor/generator and brakes, respectively. The magnitudes of these torques are controlled by the powertrain controller (command block), where internal equations reproduce the characteristic behavior of every element and implement the powertrain control algorithms.

The internal combustion engine and motor/generator are connected to a transformer MTF_1 representing the transmission and final drive. The gearbox block monitors the ICE speed and sets the gear ratio accordingly. The HEV brakes are applied right after transformer MTF_1 since the braking force is applied to the wheels. The output of the powertrain is the sum of all torques at the one junction.

On the road model side, transformer TF_2 converts the powertrain torque into a tangential force at the wheels. This force is used to propel the vehicle mass I_1 and to overcome all road resistance, being R_1 the rolling resistance and R_2 the aerodynamic drag. Road slope is modeled with an additional source of effort Se_2 that provides a force applied directly to the vehicle. Equations of control are presented in Table I. The HEV powertrains parameters were obtained from [26]–[28].

The powertrain is driven by an EUDC urban driving cycle shown in Fig. 4(a) [7]. The drive cycle speed is compared to the actual vehicle speed and the error is fed to a proportional-integral (PI) controller. This will give the appropriate command to the powertrain to obtain the desired speed. The resulting torque is shown in Fig. 4(b). Additional components can be added to this model by including the necessary elements: resistive (R), inertial (I), compliance (C), sources (Se, Sf), etc.

The dynamics of the system can be obtained by writing state equations for every energy-storing element (I and C elements). From Fig. 3, there is only one state variable (p_1) corresponding to the element I_1. Therefore, $\dot{p}_1$ can be solved.

$$\dot{p}_1 = \left(\frac{1}{r_w}\right) \cdot e(PWT) - e(R_1) - e(R_2) - Se_2 \qquad (1)$$

where the effort e(PWT) represents the powertrain torque at the output of the final drive, $\mathrm{r_w}$ is the wheel radius, $\mathrm{e(R_i)}$ the effort

TABLE I
DESIGN EQUATIONS AND PARAMETERS OF THE HEV POWERTRAIN AND ROAD MODEL

Element	Equation
MSe1	Available Torque = Max. Torque • [-2.03E-6 • (speed - 314)^2 + 1]
	Speed in rad/s | Max. Torque: 120 Nm
MSe2	Max. Motor Torque = 60 N.m | Max. Generating Torque = 110 Nm
MSe3	Max. Brake Torque = 4000 N.m
MTF1	modulus = (1 / gearbox_ratio) • (1 / final_drive)
	Ratios: 3.25/1.78/1.25/0.94/0.70 | Final dive: 3.89
TF2	modulus = r_w = 0.32 m | Wheels: 195/65 R15
I1	I1(I) = 1300 kg
R1	R1(e) = k • M • g
	k = 0.013 | M = 1300 kg | g = 9.8 m / s^2
R2	R2(e) = (1/2) • ρ • Cw • A • (f)^2
	ρ = 1.2 kg / m^3 | Cw = 0.4 | A = 2 m^2 | f = vehicle speed (m / s)
Se2	Se2(e) = M • g • sin α
	M = 1300 | g = 9.8 m / s^2 | α = 0.0°

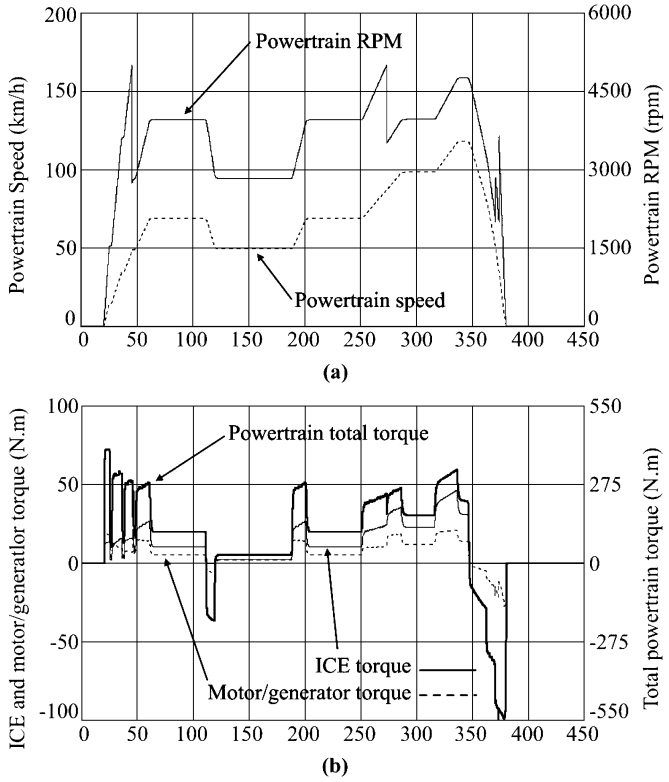

Fig. 4. Simulation of the HEV powertrain connected to a road model. (a) The engine RPM and powertrain speed, while following a drive cycle. The transmission has five gears. (b) Total torque developed by the HEV powertrain, ICE torque, and electric motor torque.

at each $\mathrm{R_i}$, $\mathrm{Se_2}$ the road slope effort and $\dot{p}_1$ is the vehicle linear momentum. Replacing each effort in (1) by its respective equation from Table I, the vehicle acceleration $\dot{\mathrm{f}}_1$ can be solved.

$$\dot{f}_1 = \left(\frac{1}{M}\right) \cdot \left[\left(\frac{1}{r_w}\right) \cdot e(PWT) - k \cdot M \cdot g - \frac{1}{2} \cdot \rho \cdot C_w \cdot A \cdot (f_1)^2 - M \cdot g \cdot \sin(\alpha)\right]. \quad (2)$$

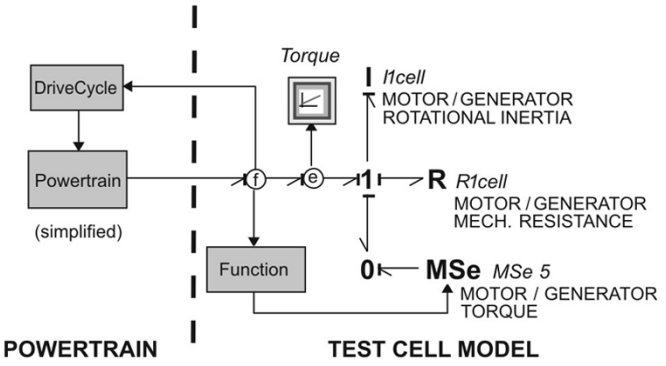

Fig. 5. Simplified HEV powertrain model connected to the motor/generator of the test cell.

From (2), it can be seen that the dynamics of the system is a function of the powertrain torque and the powertrain speed at the wheels $(\mathrm{f_1})$. The remaining parameters can be constant or time dependant. Given the input variables, the powertrain speed can be found by solving (2) for $\mathrm{f_1}$.

V. TEST CELL MODEL AND CONTROL EQUATIONS

The HEV powertrain is coupled to the test cell through an electric motor/generator. This motor/generator provides the loading to the powertrain and its torque is set by the cell controller to match the desired system's dynamics.

Since the test cell has its own dynamics, different from the road model dynamics, it is necessary to develop dynamic equations for both systems to match their response.

Fig. 5 shows the HEV powertrain connected to the motor/generator. In this case, the rotational inertia $(\mathrm{I_1cell})$ and mechanical resistance $(\mathrm{R_2cell})$ of the test cell motor/generator are much smaller compared to the resistances and inertias that the powertrain is subject to in the road model. The objective is to achieve the same dynamic response presented by (2). In this case, the motor/generator uses its torque $(\mathrm{Se_2cell})$ as variable to match the dynamics of both systems.

The HEV powertrain in Fig. 5 has been simplified and the output is the torque at the wheels, including all sources of effort: ICE, electric motor/generator and brakes. The powertrain is connected directly to the test cell model. The speed at the One Junction represents the angular speed of the powertrain.

The test cell is described with three elements, as shown in Fig. 5. The cell resistance $\mathrm{R_1cell}$ represents the mechanical losses of the motor/generator. This resistance can be constant or a function of speed. The inertia of the motor/generator is represented by $\mathrm{I_1cell}$, while its developed torque is represented by a modulated source of effort MSe. The internal equations used in this model are shown in Table II. The motor/generator parameters were obtained from [26] and [28].

The dynamics of the system depicted in Fig. 5 can be solved by writing the state equations for $\mathrm{I_1cell}$. The HEV powertrain is simplified as a source of effort with variable magnitude. The powertrain angular acceleration $\dot{\mathrm{f}}_{1\mathrm{cell}}$ can be solved.

$$\dot{f}_{1\mathrm{cell}} = \left(\frac{1}{J_{\mathrm{cell}}}\right) \cdot [e(PWT) - e(R_1\mathrm{cell}) - Se_2\mathrm{cell}]. \quad (3)$$

TABLE II
DESIGN EQUATIONS AND PARAMETERS OF THE TEST CELL MODEL

Element	Equation
I1cell	J = 0.252 kg m^2
R1cell	R = 1.2 Nm | e(R1cell) = R • f
MSe5	modulus = 1
Function	T1 = effort - 1.2 * speed - 0.252 / 1300 / 0.32 * (effort / 0.32 - 0 - 0.48 * (speed * 0.32)^2 - 0);
	if abs(165 * sign(speed)) > abs(effort / 0.32) then
	T2 = 0;
	else
	T2 = - 0.252 / 1300 / 0.32 * (- 165 * sign(speed));
	end;
	output_torque = T1 + T2;

The test cell controller will use the torque $\mathrm{Se_2cell}$ to load the HEV powertrain and match the road model dynamics described by (2). The control equation is obtained by matching the dynamic response of both systems. Therefore, the cell angular acceleration from (3) must match the angular acceleration of the powertrain from (2)

$$\dot{f}_1 = \dot{f}_{1\mathrm{cell}} \cdot r_w. \tag{4}$$

Substituting (2) and (3) to (4), $Se_2\mathrm{cell}$ can be solved.

$$Se_2\mathrm{cell} = e(PWT)\cdot\left[1-\frac{J_{\mathrm{cell}}}{m\cdot r_w^2}\right]-e(R_1\mathrm{cell})+\frac{J_{\mathrm{cell}}}{m\cdot r_w}$$
$$\cdot\left[k\cdot M\cdot g+\frac{1}{2}\cdot\rho\cdot C_w\cdot A\cdot(\dot{f}_{1\mathrm{cell}}\cdot r_w)^2+M\cdot g\cdot\sin(\alpha)\right]. \tag{5}$$

Equation (5) represents the control equation for the test cell controller. The only unknown is the torque produced by the powertrain e(PWT). The parameters related to the road model ($\mathrm{C_w}$, A, m, etc.) can be set arbitrarily, while the motor/generator parameters inertia $\mathrm{J_{cell}}$ and resistance $\mathrm{e(R_1cell)}$ can be determined from experiments and can be constant or functions of speed $\mathrm{f_1}$.

The torque produced by the powertrain can be obtained by using a torque sensor between the powertrain and the test cell motor/generator. Sensor-less operation is also possible by observing the speed from (3).

Since $\mathrm{Se_2cell}$ and $\mathrm{e(R_1cell)}$ are known at all times, speed can be observed by solving (3) for e(PWT)

$$\mathrm{e(PWT)} = J_{\mathrm{cell}}\cdot\dot{f}_{1\mathrm{cell}} + e(R_1\mathrm{cell}) + Se_2\mathrm{cell}. \tag{6}$$

The test cell is simulated in Fig. 6 with the urban driving cycle and road model presented in Fig. 3 and Table I. The exerted powertrain torque shown in Fig. 6 matches the result obtained shown in Fig. 3(b).

In order to obtain the same total powertrain torque as shown in Fig. 3(b), the motor/generator of the test cell develops a torque determined by (8) and (9). This torque is shown in Fig. 6.

The test cell is further simulated with a UDDS driving cycle [7]. The required powertrain torque and resulted test cell motor torque are shown in Fig. 7 along with the vehicle speed. It can be seen that the powertrain torque and the test cell motor torque

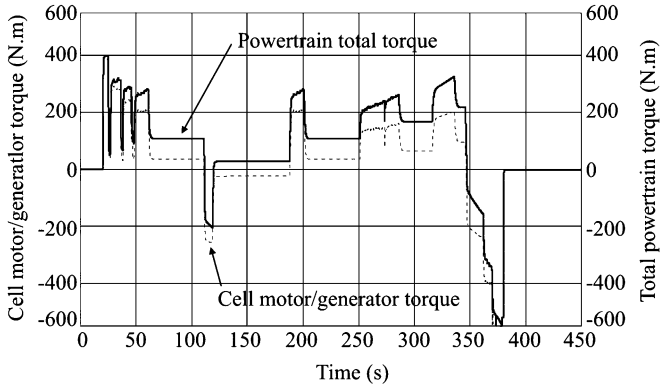

Fig. 6. Simulation of the HEV Powertrain coupled to the test cell and results of HEV powertrain torque and motor/generator exerted torque. The powertrain output torque matches the results obtained in Fig. 4(b).

are almost identical because the motor losses are negligible in these drive cycles.

VI. EXTENDED TEST CELL MODEL

The models presented in Fig. 3 and 5 can be extended to include detailed information regarding the system's dynamic response to transients. For control purposes, a higher level of information can be used to derive the controller equations and analyze system's stability and controllability.

The test cell motor/generator dynamic model depends on the type of electric machine used (i.e., permanent magnet brushless motor, squirrel cage induction motor, brush dc motor, etc.). A generalized model can be derived for all electrical machines, assuming that they all operate from a constant source of voltage and its equivalent circuit can be represented as shown in Fig. 8(a). This approximation is straightforward when using dc machines. If the motor/generator uses a time-varying source of voltage, motor control theories must be used to convert the time-varying voltages to constant sources (e.g., vector oriented control for induction machines). If this conversion is not possible, the equivalent circuit must contemplate this situation.

The Bond Graph model of the equivalent circuit is shown in Fig. 8(b). A source of effort $\mathrm{Se_1}$ represents the control voltage of the motor/generator. The windings resistance and inductance are symbolized by Rs and Ls. The remaining power from $\mathrm{Se_1}$ is

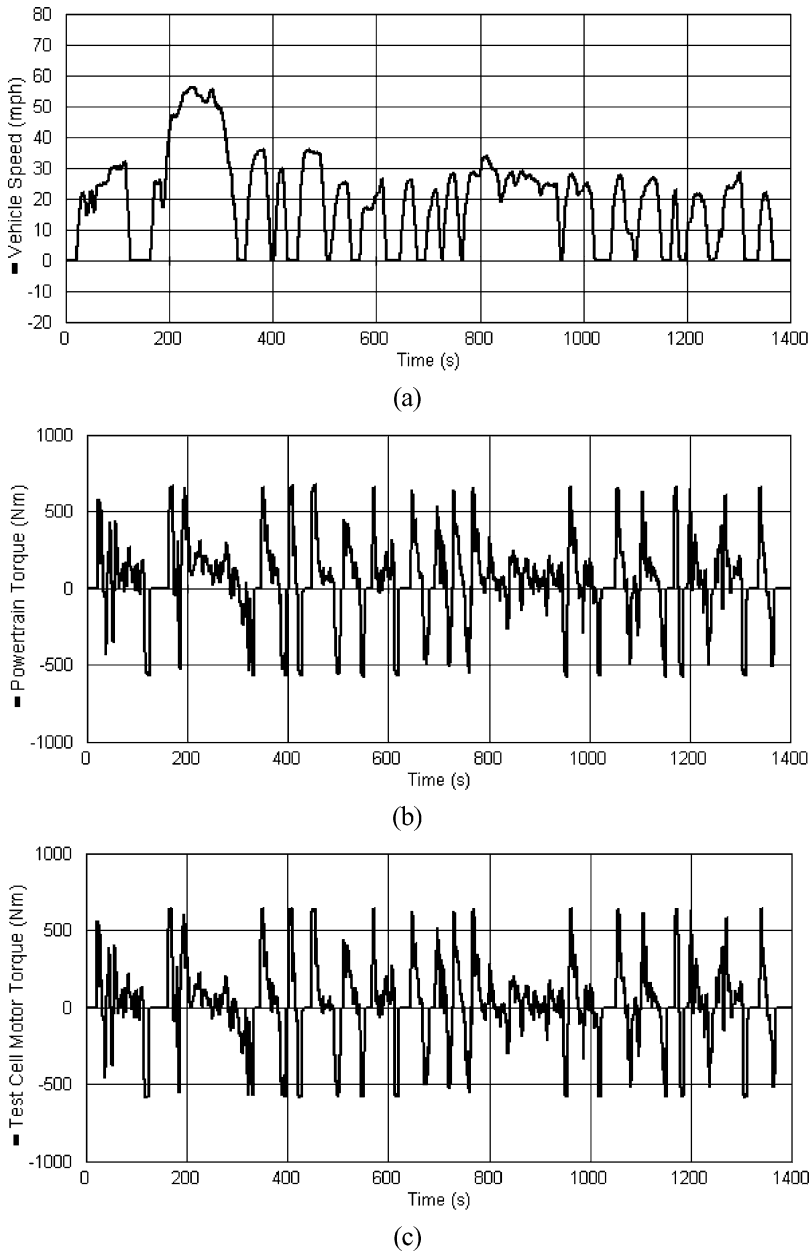

Fig. 7. Simulation of the HEV Powertrain test cell with a UDDS driving cycle. (a) Vehicle speed. (b) Required powertrain torque. (c) Resulted test cell motor torque.

transferred through a gyrator GY_1 to the mechanical domain of the motor. This gyrator produces a torque proportional to the effective current circulating through the machine's windings. This proportionality constant is usually known as the motor torque constant, often abbreviated as $\mathrm{K_T}$. The output of the gyrator (mechanical torque) is used partly to drive the machine's angular inertia J_1 and to overcome its mechanical resistance $\mathrm{R_m}$. The remaining torque goes to the test cell.

Causality analysis on the Bond Graph of Fig. 8(b) shows the mechanical inductance J_1 in derivative causality. This means that this inductance will not contribute with a state variable to the system dynamics. This derivative causality implies that the dynamics of the mechanical inertia is dependant on another state variabe, the test cell's inertia $\mathrm{I_{1cell}}$ as shown in Fig. 5. Both inertias can be added and represented by a single inertia element.

The test cell model can also include mechanical compliances (torsional deflections of shafts due to applied torque) between the powertrain and the cell motor/generator. This compliances directly affect the powertrain observed torque calculated from (6). This compliance is represented by a capacitor (C-element) in the Bond Graph model. This element may introduce instabilities to the system that might render sensor-less operation impossible.

Fig. 9 shows a complete Bond Graph model of the test cell. For dynamic analysis, the HEV powertrain should be expanded to account for individual inertias, compliances and resistances. It is also necessary to have a detailed implementation of the control algorithm and its dynamic response. Causality analysis of Fig. 9 shows that $\mathrm{C_{cell}}$ has derivative causality which represents a simulation problem since flow cannot be calculated. This simulation problem is analogous to connecting a voltage source to

TABLE III
PARAMETERS OF THE DC MOTOR AND THE INDUCTION MOTOR

DC Motor		Induction Motor	
Rated power	2.0 kW	Rated power	2.0 kW
Rated speed	1800 rpm	Rated speed	1800 rpm
Rated voltage	125 V	Rated voltage	208 V
Armature resistance	0.5 Ω	Rated frequency	60 Hz
Machine constant	0.56	Number of phases	3
Combined moment of inertia			0.06 kg. m^2
Combined resistive torque			1.6 Nm

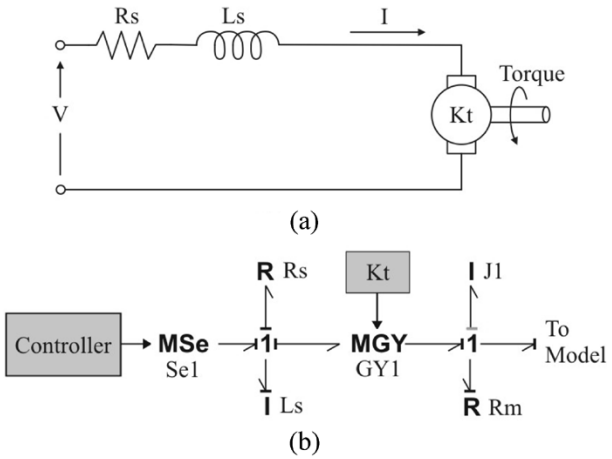

Fig. 8. (a) Simplified equivalent circuit of the test cell motor/generator. Rs and Ls are the windings resistance and inductance. R_{Fe} represents the iron loss. L_m is the magnetizing inductance. The generated torque is proportional to the current I. (b) Bond Graph model of the equivalent circuit. Note that the I-element J1 has derivative causality.

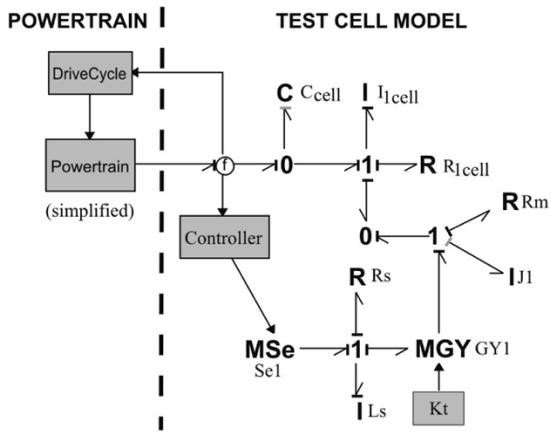

Fig. 9. Expanded Bond Graph model of the test cell, with detailed cell motor/generator model and compliance between the powertrain and test cell. Note that J1 and C_{cell} have derivative causality.

an ideal capacitor where current cannot be calculated for any given time.

To solve this causality problem, the HEV powertrain inertia has to be included in the Bond Graph model of Fig. 9, on the powertrain side and before C_{cell}. This will result in a C_{cell} element with integral causality.

VII. EXPERIMENT VERIFICATION

A scaled-down model of the powertrain test-cell was reproduced to validate the model results. Fig. 10 shows the test-cell setup, where the HEV powertrain was replaced with an induction machine. The induction machine was connected to a Brush dc motor/generator as a loading device to the powertrain. Both machines are driven by a Powerex inverter and controlled by DSpace real time controllers, respectively. The two inverters are connected to a common dc bus. The parameters of the two motors are shown in Table III.

In this setup, the induction machine has to perform motoring and generating operations similar to a HEV powertrain. A Volt-Hertz (V/Hz) control is implemented in DSpace/Matlab Simulink to drive the induction machine. The parameters of the model were determined based on the machine ratings. The input drive cycle is compared to the measured speed from the encoder and its error is fed to a PI controller. The controller adjusts the V/Hz command to the induction machine to follow the drive cycle. When the machine operates in motoring mode, power

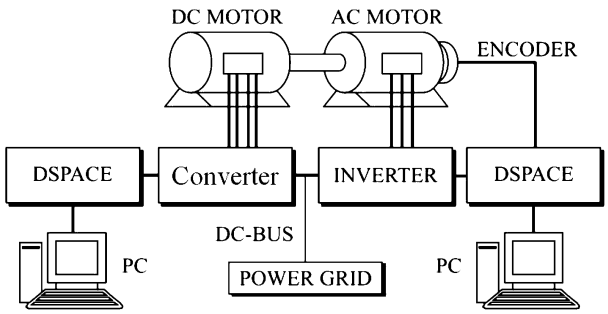

Fig. 10. The laboratory experiment setup.

will be taken from the dc bus. While operating in generating mode, the machine will deliver power to the dc bus.

The dc motor applies loading to the induction machine, according to the road model developed in Fig. 3. The proposed road model presents inertial and resistive loads to the induction machine. Since these loads are functions of speed, the speed feedback is used by the dc motor/generator controller to calculate the required load torque. The motor speed and armature current are used by the torque observer to calculate the observed powertrain torque according to (6) and the machine parameters in Table III. The observed torque and speed is used to generate a torque command, to reproduce the road load torque of Fig. 3. The resulting torque command is fed to a PI controller to adjust the dc motor armature current to achieve the necessary torque.

Fig. 11 shows the measured powertrain torque and powertrain speed. The total powertrain power has been limited to a maximum of 2 kW, corresponding to the maximum power that

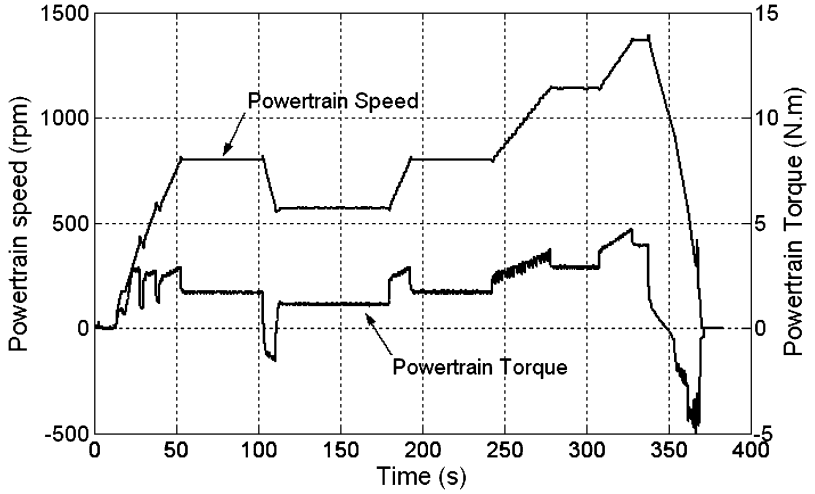

Fig. 11. Torque and speed measurements.

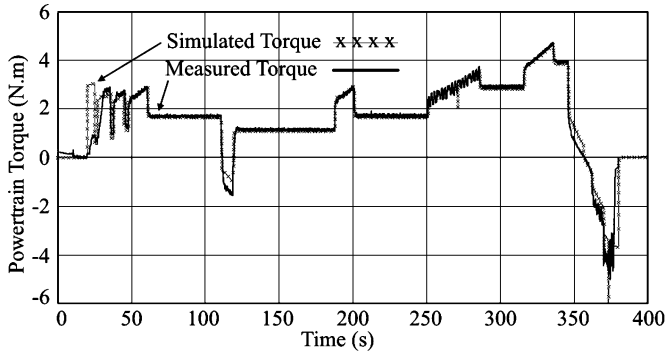

Fig. 12. Comparison of simulated powertrain torque and experiment results.

both induction and dc machines can handle. The resistive and inertial load equations of the model shown in Fig. 3 are used with scaled-down parameters. It can be seen that the powertrain speed well follows the desired driving cycle.

To validate the results of the scaled-down experiment, a simulation of the scaled-down model was performed. Fig. 12 shows a comparison between the simulated powertrain torque on the scaled-down system and the measured powertrain torque. It can be seen that the measured torque matches the simulated torque except at some transient point. We believe that the error is caused by the inaccuracy of the experiment model which includes inertia and resistive torque measurements.

VIII. Conclusion

This paper proposed an HEV powertrain test cell capable of producing various loading conditions, including positive and negative resistive and inertial loads of any magnitude, avoiding the use of mechanical inertial loads involved in conventional test cells. The test cell was modeled using Bond Graphs. The modeling method enables rapid modeling and extraction of control equations to achieve programmable loading conditions.

By modeling the powertrain and test cell with Bond Graphs, modeling problems were detected by causality analysis on the power bonds. These problems were solved by modifying the model where needed and improving the simulation results. These models can be exported to a block diagram model suitable for simulation in Matlab/Simulink. Block diagrams in this software also enables rapid implementation on DSP/DSpace real time controllers. Experiment results added confidence to the proposed model.

The proposed test cell is capable of testing both series and parallel HEV powertrains. The developed algorithm through the use of Bond Graphs enables the test cell capable of reproducing a predetermined driving cycle with sufficient accuracy and repeatability in multiple control modes.

References

[1] C. C. Chan and K. T. Chau, *Modern Electric Vehicel Technology*. Oxford, U.K.: Oxford University Press, 2001.

[2] K. Muta, M. Yamazaki, and J. Tokieda, "Development of new-generation hybrid system THS II—drastic improvement of power performance and fuel economy," in *SAE World Congress*, Detroit, MI, Mar. 8–11, 2004, SAE Paper Number 2004-01-0064.

[3] K. Butler, M. Ehsani, and P. Kamath, "A Matlab-based modeling and simulation package for electric and hybrid electric vehicle design," *IEEE Trans. Veh. Technol.*, vol. 48, no. 6, pp. 1770–1778, Nov. 1999.

[4] B. Baumann, G. Washington, B. Glenn, and G. Rizzoni, "Mechatronics design and control of hybrid electric vehicles," *IEEE/ASME Trans. Mechatronics*, vol. 5, no. 1, pp. 58–72, Mar. 2000.

[5] X. He and J. Hodgson, "Modeling and simulation for hybrid electric vehicles—part I," *IEEE Trans. Transport. Syst.*, vol. 3, no. 4, pp. 235–243, Dec. 2002.

[6] ——, "Modeling and simulation for hybrid electric vehicles—part II," *IEEE Trans. Transport. Syst.*, vol. 3, no. 4, pp. 244–251, Dec. 2002.

[7] ADVISOR 2004—Virtual Vehicle Analysis (2005, Feb. 1). *http://www.avl.com/advisor* [Online]

[8] J. Clayton Jr. *et al.*, "Dynamometer for simulating the inertial and road load forces encountered by motor vehicles and method," USPTO Patent 6 247 357, Jun. 2001.

[9] M. Fleming, G. Len, and P. Stryker, "Design and construction of a university-based hybrid electric powertrain test cell," in *Future Transport. Technol. Conf.*, Costa Mesa, CA, Aug. 21–23, 2000, SAE Paper Number: 2000-01-3106.

[10] P. Karnopp, P. Margolis, and P. Rosenberg, *System Dynamics: Modeling and Simulation of Mechatronics Systems*. New York: Wiley Interscience, 2000.

[11] J. Kim and M. Bryant, "Bond graph model of a squirrel cage induction motor with direct physical correspondence," *ASME J. Dynam. Syst., Measure., Contr.*, vol. 122, pp. 461–469, Sep. 2000.

[12] H. Fraisse, J. P. Masson, F. Marthouret, and H. Morel, "Modeling of a nonlinear conductive magnetic circuit. 2. Bond graph formulation," *IEEE Trans. Magnetics*, vol. 31, pp. 4068–4070, Nov. 1995.
[13] D. Landen, "Analysis of electromagnetic systems using the extended bond graph method: mechanically static systems," *IEEE Trans. Magnetics*, vol. 39, pp. 491–497, Jan. 2003.
[14] S. Xia, D. A. Linkens, and S. Bennett, "Automatic modeling and analysis of dynamic physical systems using qualitative reasoning and bond graphs," *Intelligent Systems Eng.*, vol. 2, pp. 201–212, Autumn 1993.
[15] G. L. Gissinger, Y. Chamaillard, and T. Stemmelen, "Modeling a motor vehicle and its braking system," *J. Math. Comput. Simulation*, vol. 39, pp. 541–548, 1995.
[16] K. Suzuki and S. Awazu, "Four-track vehicles by bond graph-dynamic characteristics of four-track vehicles in snow," in *26th Ann. Conf. IEEE Ind. Electron. Soc., IECON 2000*, vol. 3, Oct. 2000, pp. 1574–1579.
[17] J.-H. Kim and D.-I. Dan Cho, "An automatic transmission model for vehicle control," in *IEEE Conf. Intelligent Transport. Syst., ITSC 97*, Nov. 1997, pp. 759–764.
[18] N. Nishijiri, N. Kawabata, T. Ishikawa, and K. Tanaka, "Modeling of ventilation system for vehicle tunnels by means of bond graph," in *26th Annual Conf. IEEE Ind. Electron. Soc., IECON 2000*, vol. 3, Oct. 2000, pp. 1544–1549.
[19] M. L. Kuang, M. Fodor, D. Hrovat, and M. Tran, "Hydraulic brake system modeling and control for active control of vehicle dynamics," in *Proc. 1999 Amer. Contr. Conf.*, vol. 6, Jun. 1999, pp. 4538–4542.
[20] M. Khemliche, I. Dif, S. Latreche, and B. O. Bouamama, "Modeling and analysis of an active suspension 1/4 of vehicle with bond graph," in *Proc. First Int. Symp. Contr., Commun. Signal*, Mar. 2004, pp. 811–814.
[21] A. J. Truscott and P. E. Wellstead, "Bond graphs modeling for chassis control," in *IEE Colloq. Bond Graphs in Control*, Apr. 1990, pp. 5/1–5/2.
[22] N. Coudert, G. Dauphin-Tanguy, and A. Rault, "Mechatronic design of an automatic gear box using bond graphs," in *Int. Conf. Syst., Man Cybern.*, Oct. 17–20, 1993, pp. 216–221.
[23] D. Jaume and J. Chantot, "A bond graph approach to the modeling of thermics problems under the hood," in *Int. Conf. Syst., Man Cybern.*, Oct. 17–20, 1993, pp. 228–233.
[24] J. Meng, Z. Zhen, G. Biswas, and N. Sarkar, "Hybrid fault adaptive control of a wheeled mobile robot," *IEEE/ASME Trans. Mechatronics*, vol. 8, pp. 226–233, Jun. 2003.
[25] G. A. Hubbard and K. Youcef-Toumi, "Modeling and simulation of a hybrid-electric vehicle drivetrain," in *Proc. 1997 Amer. Contr. Conf.*, vol. 1, Jun. 4–6, 1997, pp. 636–640.
[26] R. Bosch, *Automotive Handbook*, 5th ed: Bentley, 2000.
[27] J. Heywood, *Internal Combustion Engine Fundamentals*, 1st ed. New York: McGraw-Hill, 1988.
[28] H. Ogawa, M. Matsuki, and T. Eguchi, Development of a power train for the hybrid automobile—The civic hybrid, 2003.

Mariano Filippa (S'03) received the B.S.M.E. degree from the Technological Institute of Buenos Aires (ITBA), Buenos Aires, Argentina.

He is currently with General Electric Inc., Motion Systems and Controls, Salem, VA. He is responsible of developing applications for Electric/Hybrid Vehicles and Wind Power Pitch Control. He joined the University of Michigan, Dearborn, in 2002 as graduate student and a Research Assistant working at the DTE Power Electronics Laboratory. He was responsible for the design of power electronic converters and testing equipment for motor control applications and laboratory testing. From 2001 to 2002, he was an Application Engineer with Asea Brown Boveri (ABB), Buenos Aires, working in the area of robotics. He had a key role in the engineering and construction of a fully automated robotized palletizing cell for the consumer industry. During 2002 , he was also involved in R&D with the Technological Institute of Buenos Aires, designing a distributor-less ignition system for laboratory research. His research interests are in low and medium power electronics applications, ranging from control algorithms, EMI reduction and equipment design, and testing in the areas of motor control and hybrid vehicle applications.

Dr. Filippa has been a student member of ASME since 2000.

Chunting Mi (S'00–A'01–M'01–SM'03) received the B.S.E.E. and M.S.E.E. degrees from Northwestern Polytechnical University, Xi'an, Shaanxi, China, and the Ph.D. degree from the University of Toronto, Toronto, ON, Canada, all in electrical engineering.

He is an Assistant Professor with the University of Michigan, Dearborn, with teaching responsibilities in the area of power electronics, electric vehicles, electric machines and electric drives. He joined General Electric Canada Inc. Peterborough, ON, as an Electrical Engineer in 2000, where he was responsible for designing and developing large electric motors and generators. He was with the Rare-Earth Permanent Magnet Machine Institute of Northwestern Polytechnical University, from 1988 to 1994. He joined Xi'an Petroleum Institute, Xi'an, as an Associate Professor and Associate Chair of the Department of Automation in 1994. He was a visiting scientist with the University of Toronto from 1996 to 1997. He has recently developed a Power Electronics and Electrical Drives Laboratory at the University of Michigan, Dearborn. His research interests are electric drives, power electronics, induction motors, brushless motors, and PM synchronous machines; renewable energy systems; electrical and hybrid vehicle powertrain design and modeling.

Dr. Mi is the Chair of the Power Electronics and Industrial Electronics Chapter, and the Director of Educational Activities of the IEEE Southeast Michigan Section. He is the recipient of the 2005 Distinguished Teaching Award, University of Michigan, Dearborn.

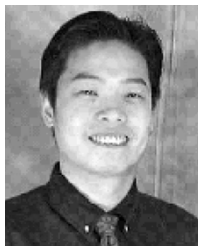

John Shen (S'90–M'95–SM'03) received the B.S.E.E. degree from Tsinghua University, Beijing, China, in 1987, and the M.S. and Ph.D. degrees both in electrical engineering from Rensselaer Polytechnic Institute, Troy, NY, in 1991 and 1994, respectively.

He is an Associate Professor of Electrical Engineering with the University of Central Florida (UCF), Orlando. Between 1994 and 1999, he held a variety of positions including Senior Principal Staff Scientist with Motorola Semiconductor Products Sector, Phoenix, AZ. He was with the University of Michigan, Dearborn, as an Assistant and Associate Professor with the Department of Electrical and Computer Engineering between 1999 and 2003. His research areas include power electronics, power semiconductor devices, and ICs, power management for computers and telecom equipment, automotive electronics, renewable and alternative energy systems, and electronics manufacturing. He has published more than 60 journal and conference articles, and holds eight issued and many pending U.S. patents in these areas.

Dr. Shen is a recipient of the 2003 NSF CAREER Award, the 2003 IEEE Best Automotive Electronics Paper Award from IEEE Society of Vehicular Technology, and the 1996 Motorola Science and Technology Award. He serves as the Automotive Power Electronics Technical Committee Chair and at-large AdCom member of the IEEE Power Electronics Society. He also serves as the co-Guest Editor of the 2006 Special Issue on Automotive Power Electronics of IEEE TRANSACTIONS IN POWER ELECTRONICS.

Randy C. Stevenson received the B.S. and Ph.D. degrees in physics, from the University of Michigan, Ann Arbor, in 1974 and 1982, respectively.

He is currently with Visteon Corporation, Dearborn, MI, working in the Powertrain Division, where he develops electromagnetic FEA and system models for ignition system components. While at Visteon, he has also worked on the development of a molten solder dispensing system, as well as electromagnetic retarder braking systems, and an electric motor all-wheel drive system. He previously worked for Bell Laboratories, North Andover, MA, on nuclear-generated high-altitude EMP threats to the telephone system, and the design and development of surface acoustic wave devices for retiming for optical fiber transmission. He has also worked for KMS Fusion, formally of Ann Arbor, on the optical characterization of laser fusion targets, and for Ford Research Labs, Dearborn, on engine misfire detection, and the application of fuzzy logic to the car-following problem. He has been an Adjunct Professor at the University of Michigan, Dearborn, where he has taught graduate course in control theory, and undergraduate course in physics.